Lignin impairs Cel7A degradation of in vitro lignified cellulose by impeding enzyme movement and not by acting as a sink

Zachary K. Haviland[1], Daguan Nong[1], Nerya Zexer[2], Ming Tien[3], Charles T. Anderson[2], William O. Hancock[*1,4]

[1] Department of Biomedical Engineering, Pennsylvania State University, University Park, Pennsylvania, USA

[2] Department of Biology, Pennsylvania State University, University Park, Pennsylvania, USA

[3] Department of Biochemistry and Molecular Biology, Pennsylvania State University, University Park, Pennsylvania, USA

[4] Department of Chemistry, Pennsylvania State University, University Park, Pennsylvania, USA

* Corresponding author. **Email:** woh1@psu.edu

Abstract

Background: Cellulose degradation by cellulases has been studied for decades due to the potential of using lignocellulosic biomass as a sustainable source of bioethanol. In plant cell walls, cellulose is bonded together and strengthened by the polyphenolic polymer, lignin. Because lignin is tightly linked to cellulose and is not digestible by cellulases, is thought to play a dominant role in limiting the efficient enzymatic degradation of plant biomass. Removal of lignin via pretreatments currently limits the cost-efficient production of ethanol from cellulose, motivating the need for a better understanding of how lignin inhibits cellulase-catalyzed degradation of lignocellulose. Work to date using bulk assays has suggested three possible inhibition mechanisms: lignin blocks access of the enzyme to cellulose, lignin impedes progress of the enzyme along cellulose, or lignin binds cellulases directly and acts as a sink.

Results: We used single-molecule fluorescence microscopy to investigate the nanoscale dynamics of Cel7A from *Trichoderma reesei*, as it binds to and moves along purified bacterial cellulose in vitro. Lignified cellulose was generated by polymerizing coniferyl alcohol onto purified bacterial cellulose, and the degree of lignin incorporation into the cellulose meshwork was analyzed by optical and electron microscopy. We found that Cel7A preferentially bound to regions of cellulose where lignin was absent, and that in regions of high lignin density, Cel7A binding was inhibited. With increasing degrees of lignification, there was a decrease in the fraction of Cel7A that moved along cellulose rather than statically binding. Furthermore, with increasing lignification, the velocity of processive Cel7A movement decreased, as did the distance that individual Cel7A molecules moved during processive runs.

Conclusions: In an in vitro system that mimics lignified cellulose in plant cell walls, lignin did not act as a sink to sequester Cel7A and prevent it from interacting with cellulose. Instead, lignin

both blocked access of Cel7A to cellulose and impeded the processive movement of Cel7A along cellulose. This work implies that strategies for improving biofuel production efficiency should target weakening interactions between lignin and cellulose surface, and further suggest that nonspecific adsorption of Cel7A to lignin is likely not a dominant mechanism of inhibition.

Introduction

Biofuels are a renewable energy source that can assist in the transition to a low-carbon economy as the world faces the dual challenges of climate change and increasing energy demand (1, 2). Cellulose and lignin, two of the most abundant biopolymers found in nature, are structural components of the plant cell wall that have become targets for biofuel production, with a variety of strategies being implemented to convert these two substrates into usable forms of energy (2-4). Cellulose is a homopolymer of β-1,4-linked glucose units, with parallel glucan chains bonding to form partially crystalline microfibrils (5, 6). Lignin is a polyphenolic polymer generated by radical coupling of monolignols that interacts tightly with cellulose in the cell wall (7, 8). Cellulosic biomass can be converted into biofuels after deconstruction by cellulases and fermentation of the resulting glucose (4, 9). However, enzymatic cellulose degradation is currently inefficient due to both the limited accessibility of cellulose chains when packed into a crystalline lattice, and obstruction by other cell wall components such as lignin, hemicellulose, and pectin (10-13). Lignin cannot be hydrolyzed by cellulases, making plant biomass recalcitrant to enzymatic digestion, but the mechanisms by which lignin impedes cellulase activity are poorly understood (14-19). In current schemes for biofuel production, lignin is removed from cellulosic biomass by thermochemical and acidic pretreatments that are costly and reduce the feasibility, scalability, and

sustainability of the process (20-23). Thus, understanding how lignin inhibits the degradation of cellulose by cellulases is crucial for optimizing biofuel production from lignocellulose.

A model cellulase used to study cellulose degradation is the cellobiohydrolase I, Cel7A. *Tr*Cel7A is a processive exoglucanase from *Trichoderma reesei* (teleomorph *Hypocrea jecorina*) that binds to the reducing end of cellulose chains. Its catalytic domain hydrolyzes the glycosidic bonds in cellulose, releasing the disaccharide cellobiose as a product, while the cellulose binding module is thought to bind to crystalline cellulose and thus enhance enzyme affinity (6, 24, 25). Removal of lignin from plant-derived lignocellulose improves the rate of cellulose degradation in bulk assays (13, 19, 26). Similarly, polymerizing lignin onto isolated cellulose *in vitro* decreases the bulk cellulase activity (26-29). These and other prior studies have posited three potential mechanisms (shown in Fig. 1) by which lignin inhibits cellulose degradability: 1) lignin might physically block the initial binding of Cel7A to the cellulose surface through the catalytic domain, the carbohydrate binding domain, or both (13, 30); 2) lignin might impede the processive catalysis of Cel7A bound to cellulose, effectively acting as a roadblock (31); 3) lignin might act as a "sink" for Cel7A by irreversibly adsorbing the enzyme through the catalytic domain, the cellulose binding module, or both (29, 32-34). Thus, although there is general agreement that lignin inhibits cellulase activity, the precise mechanism of inhibition and the best strategy for relieving this inhibition are not clear.

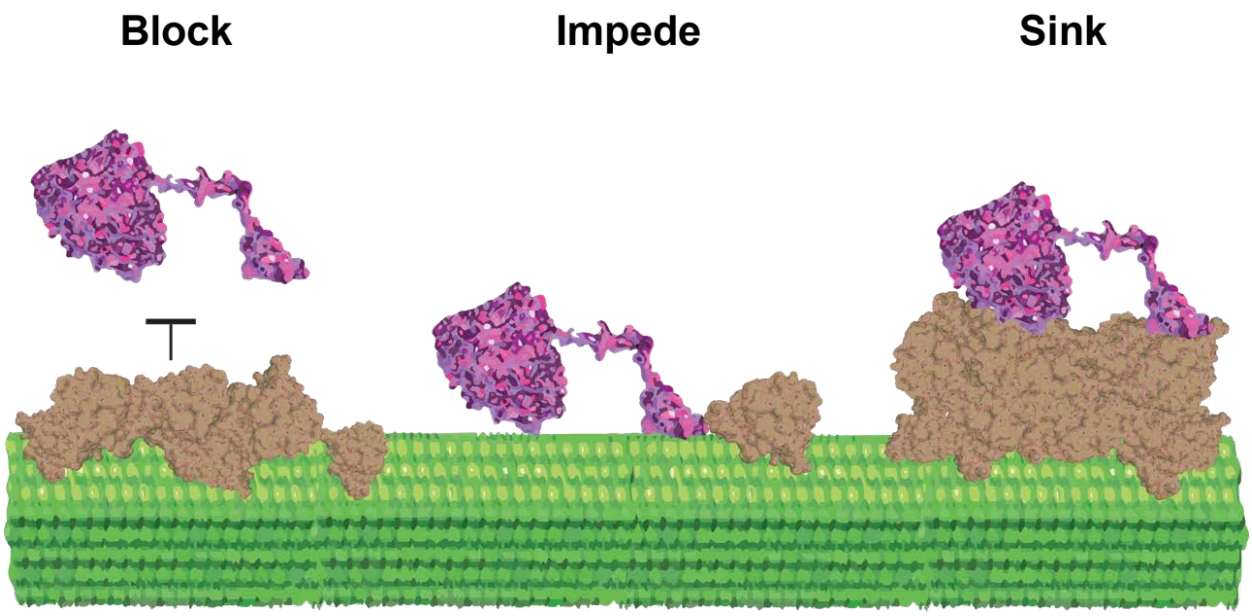

Figure 1: Potential inhibition mechanisms. Lignin may inhibit Cel7A on cellulose by blocking binding of enzymes to cellulose, by impeding the progress of enzymes bound to cellulose, or by acting as a sink by nonspecifically adsorbing enzymes.

One shortcoming in the field is that most prior analyses of cellulase inhibition by lignin lack direct observations of the interaction between lignin and cellulases (13, 19, 26, 28, 29). However, direct visualization of cellulase enzymes is possible using single-molecule microscopy (31, 35). We have constructed a high-resolution microscope that can track, at nanometer resolution, thousands of individual Cel7A molecules performing cellulose degradation on immobilized cellulose (36). We found that Cel7A reversibly transitions between free diffusion in solution, static binding to cellulose, and processive movement along cellulose (37). Here, we extended this single-molecule fluorescence approach to test potential molecular mechanisms by which lignin inhibits cellulose degradation by Cel7A. Synthetic analogs of plant cell walls were constructed by polymerizing G-lignin *in vitro* onto bacterial cellulose at varying lignin-to-cellulose ratios (38). This approach eliminates potential effects of other wall components like hemicellulose and pectin,

allowing us to focus only on lignin bound to cellulose. The resulting lignified cellulose also serves as a model of pretreated native lignocellulose that is used industrially. We asked the following three questions: 1) Does lignin deposition on cellulose inhibit Cel7A binding to the cellulose surface? 2) Does lignin alter Cel7A dynamics during processive movement along cellulose? 3) Does Cel7A accumulate on lignin due to irreversible binding?

Using a combination of scanning electron microscopy (SEM) and interference reflection microscopy (IRM), we found that *in vitro*-polymerized lignin formed structures that enclose cellulose strands and that Cel7A binding to lignified cellulose was negatively correlated with lignin. Using total internal reflection fluorescence microscopy (TIRFM), we quantified the dynamics of quantum dot-labeled Cel7A molecules and found that lignin decreased the fraction of moving enzymes, as well as their run lengths and velocities. These data are inconsistent with lignin acting as a sink that irreversibly binds Cel7A. Instead, the data indicate that lignin inhibits Cel7A by blocking its initial interaction with the cellulose surface and by impeding the progress of moving Cel7A molecules.

Results

In vitro polymerized lignin occludes the surface of cellulose

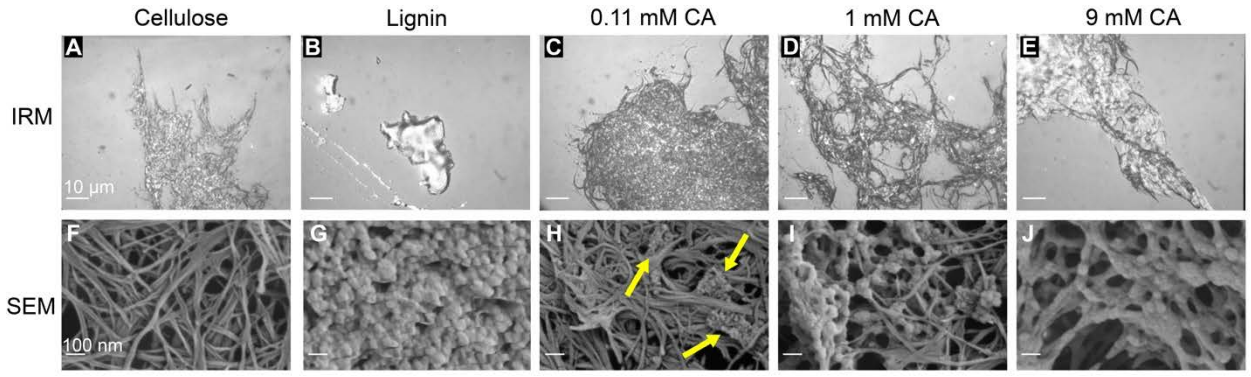

Figure 2: Morphology of lignin polymerized with acetobacter cellulose *in vitro*. First column: cellulose only; second column: lignin only; third through fifth columns: cellulose with lignin polymerized from increasing concentrations of coniferyl alcohol (CA). Top row are images from interference reflection microscopy (IRM), scale bars = 10 μm. Bottom row are images from scanning electron microscopy (SEM), scale bars = 100 nm. An additional image with lignin highlighted in false colored is provide in Fig. S2.

To examine how lignin alters cellulose degradation by Cel7A, we created lignified cellulose by depositing lignin onto *Acetobacter* cellulose *in vitro* using a mixture of coniferyl alcohol, hydrogen peroxide and horseradish peroxidase (38). To vary the degree of lignification, the reaction contained 4.25 mM cellulose and between 0.11 mM and 9 mM coniferyl alcohol and hydrogen peroxide. Hereafter, the CA concentrations added to the reactions are used to differentiate the lignin samples. To assess the relative coverage of the cellulose by lignin, we first examined samples by interference reflection microscopy (IRM) (39, 40). Flow cells were created using a plasma-cleaned coverslip and a microscope slide, and the lignocellulose samples were dried in the flow cell to adhere to the coverslip before being rehydrated with buffer. Under IRM, the cellulose-only sample showed large tangles of cellulose strands with the strands becoming sparser around the edges of the cellulose masses, allowing smaller cellulose bundles to be visualized (Fig. 2A). In contrast, in the lignin-only sample, large aggregates of lignin were visible that had much more contrast than the cellulose samples and had a smooth morphology under IRM compared to the rough surface of the cellulose (Fig. 2B). By IRM, the 0.11 mM and 0.33 mM CA samples were indistinguishable from the cellulose-only controls (Fig. 2C and Fig. S1D), but at concentrations of 1 mM CA and higher, the lignin was visible under IRM as small round aggregates dispersed across the cellulose surface (Fig. 2D). At the highest CA concentration of 9

145 mM, large patches of lignin covered significant portions of the cellulose surface and appeared to
146 be integrated between the cellulose strands (Fig. 2E).
147
148 Next, we used scanning electron microscopy (SEM) to probe the nanostructure of the
149 synthetic lignocellulose. The cellulose-only sample showed fibrils of various widths and lengths
150 that formed an intricate meshwork with varying depths (Fig. 2F). In contrast, the lignin-only
151 sample appeared as a mass of globular structures that created a rough surface with no clear
152 organization (Fig. 2G). In the 0.11 mM CA sample, nanoscale cauliflower-like lignin aggregates
153 were intertwined in the cellulose strands as indicated by yellow arrows in Figure 2H; increasing
154 aggregate densities were observed in the 1 mM sample with some aggregates on the cellulose
155 surface and others entangled in the cellulose meshwork (Fig. 2I). In the 9 mM CA sample, some
156 lignin patches encased regions of cellulose, and in some instances appeared to constrict multiple
157 cellulose strands into larger bundles (Fig. 2J). It should be noted that the deposition of lignin onto
158 cellulose was heterogenous, with some areas of cellulose having more lignin than other areas in
159 the same sample (Fig. S2). Together, these results establish that increasing concentrations of CA
160 result in both greater amounts of lignin deposition on cellulose and different lignocellulose
161 morphologies.
162
163 **Cel7A does not preferentially accumulate on *in vitro* polymerized lignin**

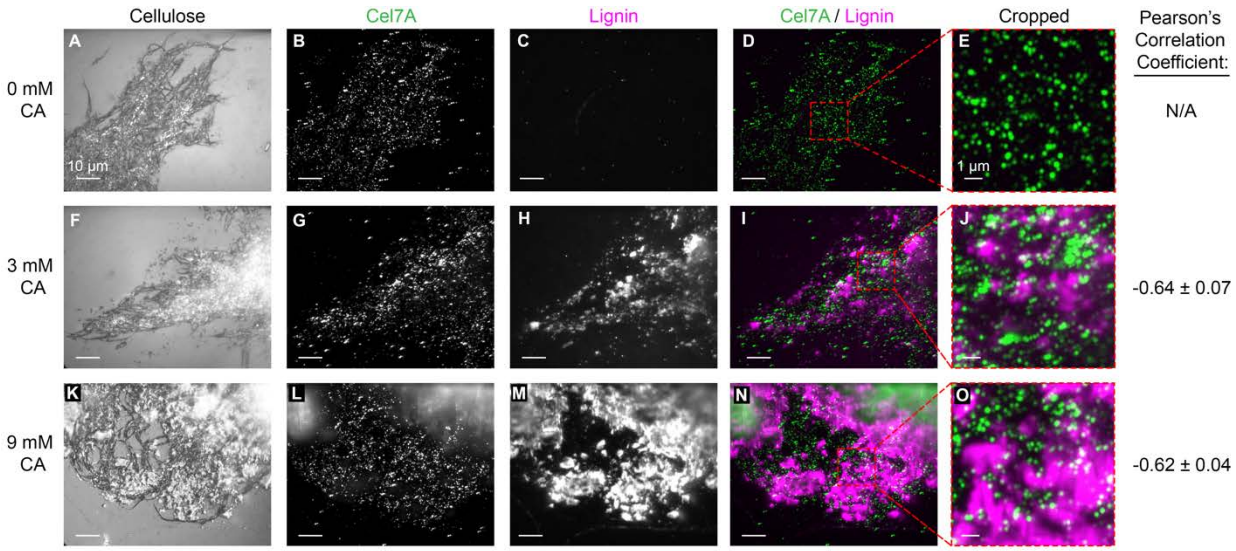

Figure 3: Cel7A enzymes bind to immobilized cellulose but not to lignin. First column: interference reflection microscopy images of synthetic lignocellulose immobilized on a glass coverslip. Second column: total internal reflection fluorescence microscopy images of Qdot-labeled Cel7A as they bind to cellulose over 500 seconds. Third column: lignin fluorescently stained by the lignin dye Basic Fuchsin. Fourth column: overlay of Qdot-labeled Cel7A (green) and lignin (magenta) images. Fifth column: cropped regions of the overlay images shown in the fourth column. For columns 1-4: scale bar = 10 µm. For column 5: scale bar = 1 µm.

The first question we addressed was the degree to which Cel7A directly interacts with lignin. On one hand, lignin might physically block binding of Cel7A to cellulose (Fig. 1, left) (13, 30). On the other hand, lignin may act as a "sink" by nonspecifically binding Cel7A and thus indirectly preventing the enzyme from interacting with cellulose (Fig. 1, right) (29, 32-34). To test these competing hypotheses, we visualized the locations of Cel7A binding events on the immobilized cellulose and compared them to the position of the deposited lignin. Experiments were carried out at 21°C in 50 mM sodium acetate buffer, pH 5.0. We focused our analysis on the 3 mM and 9 mM samples that contained micron-scale lignin patches that were considerably larger than the ~300 nm point-spread-function of the microscope (36). Cellulose was imaged with IRM,

Cel7A labeled with quantum dots (Qdots) were introduced, and the binding events on lignocellulose were recorded for 500 seconds using total internal reflection fluorescence microscopy (TIRFM) (37). Following a washout of the Cel7A with buffer, the lignin-specific dye Basic Fuchsin (41) was washed in and the location of the lignin was imaged by TIRFM. Finally, the image of fluorescently labeled lignin was overlayed with a maximum projection of the Cel7A video to show the binding locations for all the molecules in each video (Fig. 3).

We next compared the sites of Cel7A binding with the position of the deposited lignin. In the cellulose-only samples, no visible Basic Fuchsin fluorescence was observable (Fig. 3C), and the Cel7A binding density was relatively uniform across the immobilized cellulose (Fig. 3B). In the 3 mM CA samples, small patches and puncta of lignin were visible (Fig. 3H), and large patches of lignin were apparent in the 9 mM CA samples (Fig. 3M). In overlay images, few Cel7A molecules appeared to co-localize with lignin (Fig. 3I and Fig. 3N). To more quantitatively assess the spatial correlation between Cel7A and lignin, we used an ImageJ plug-in that compares the fluorescent intensities of different fluorescent channels for each pixel and calculates a Pearson's correlation coefficient (42). A "sink" model predicts a positive correlation with +1 denoting perfect co-localization, a "blocking" model predicts a negative correlation with -1 denoting perfect anticorrelation, and zero correlation is predicted if lignin has no effect on Cel7A binding to cellulose (43). An average Pearson's correlation coefficient of -0.638 ± 0.068 (mean ± SD, N = 3 experiments) was calculated for the 3 mM CA samples and a -0.615 ± 0.037 (mean ± SD, N = 3 experiments) coefficient was calculated for the 9 mM CA samples. From these negative correlations, we conclude that with our experimental conditions in this *in vitro* environment, lignin

does not act as a "sink" by nonspecifically binding Cel7A. Instead, the data are consistent with lignin blocking the binding of Cel7A to cellulose.

To conclude this analysis, we carried out two control experiments. First, we tested whether polymerization of lignin onto cellulose changes its Cel7A binding properties. To test this question, we polymerized lignin in the absence of cellulose and then combined this pure lignin with pure (unlignified) cellulose in a flow cell and measured Cel7A binding. We again found that there was little Cel7A binding to the lignin and clearly preferential binding to the cellulose (Fig. S3). As a final control to test whether bovine serum albumin (BSA) used to block nonspecific binding from the glass surface was blocking Cel7A binding to lignin, we repeated the experiment without adding BSA to the solutions. In the absence of BSA the correlation of cellulose and lignin binding was 0.037, indicating the Cel7A bound to a similar extent to cellulose and lignin (Fig. S4). Thus, in the absence of blocking protein, Cel7A can non-specifically bind to lignin, but even in this case the near-zero correlation indicates that lignin does not act as a preferential sink for binding Cel7A.

***In vitro* polymerized lignin impedes Cel7A motion on cellulose**

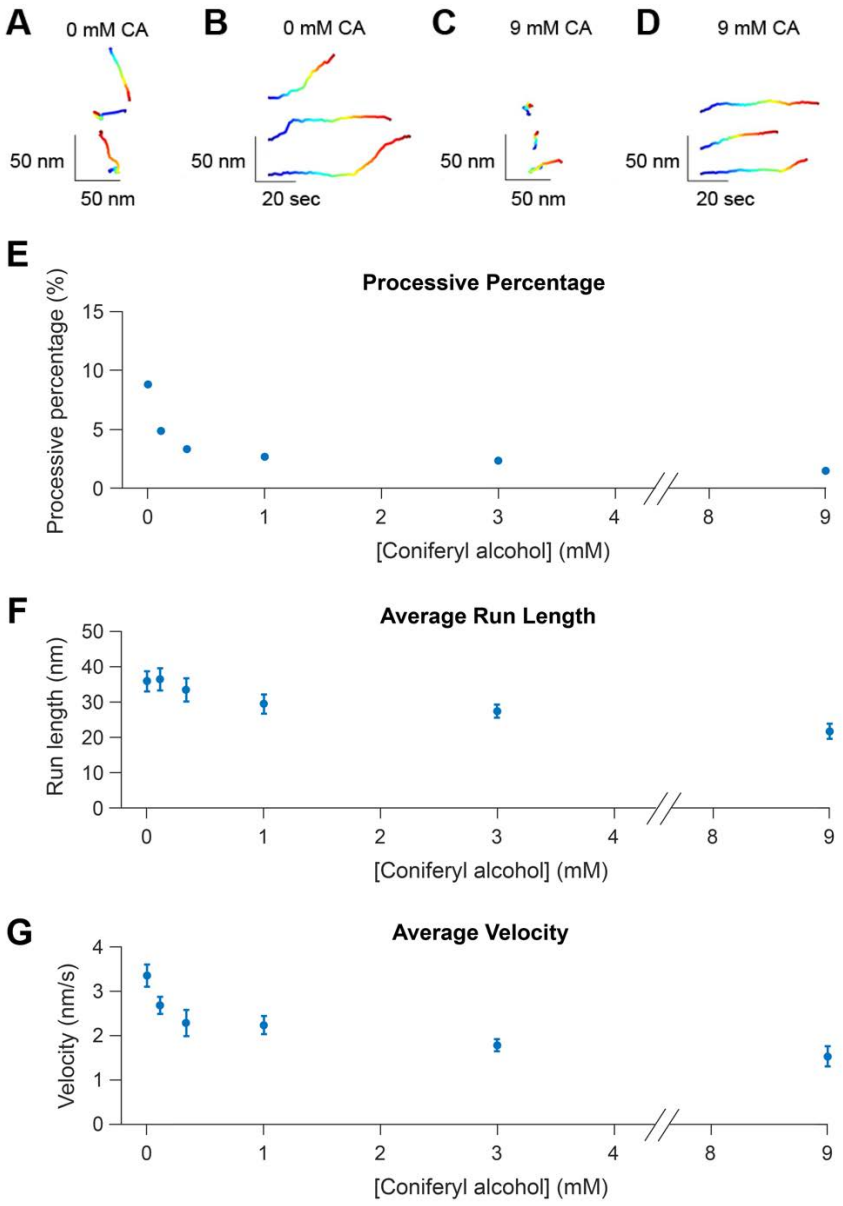

Figure 4: Cel7A molecules display diminishing processive behavior on cellulose with increasing lignification. Qdot-labeled Cel7A enzymes were imaged using total internal reflection microscopy at 1 frame/second and positions were fit using a Gaussian point-spread function. A: X-Y positions over time for three different Cel7A enzymes on lignin-free cellulose. B: Distance from origin versus time for the same three Cel7A enzymes on lignin-free cellulose shown in A. C: X-Y positions over time for three different Cel7A enzymes on lignocellulose prepared using 9 mM CA. D: Distance from origin versus time for the same three Cel7A enzymes on lignocellulose prepared using 9 mM CA shown in C. For all traces, blue represents the start of the binding event and red indicates the end of the binding event. E: Percentage of the total Cel7A enzymes imaged that displayed processive behavior. F: Average run length of

processive segments; runs less than 10 nm long were excluded from analysis. G: Average velocity of processive segments; velocities less than 0.1 nm/s were excluded from analysis. Run lengths and velocities are presented as mean +/- SEM. The number of enzymes tracked for each sample were: 0 mM CA, N = 224; 0.11 mM CA, N = 172; 0.33 mM CA, N = 154; 1 mM CA, N = 93; 3 mM CA, N = 88; 9 mM CA, N = 56.

To assess how lignin alters the behavior of Cel7A on cellulose, single-molecule fluorescence imaging was used to track quantum dot-labeled Cel7A molecules binding to and moving along immobilized lignocellulose. Videos were recorded at 1 frame/s for 1000 s and the resulting trajectories of individual particles were tracked by fitting a 2D gaussian distribution to the point-spread function of the quantum dots in every frame using the program FIESTA (44). To subtract stage drift, TetraSpeck beads were non-specifically fixed to the glass surface and used as fiduciary markers (36). The resulting drift-corrected trajectories were analyzed using a custom-made MATLAB code that plots both X-Y positions and the distance traveled from the origin versus time. Many of the tracked molecules remained static, defined as a displacement of less than 10 nm from the original location over the duration of a binding event. Other molecules displayed processive segments, defined as the enzyme moving continuously for at least 5 s for a distance of at least 10 nm. A minimum velocity of 0.1 nm/s was applied to the analysis to differentiate processive movement from stage drift that was not fully corrected. Exemplary traces of X-Y positions for processive molecules, as well as plots displaying the distance from the origin over time, are shown in Figure 4A-D.

To characterize enzyme activity, we quantified the fraction of Cel7A molecules that moved processively, along with the velocities and run lengths of the processive moving enzymes. The percentage of processive molecules decreased with increasing amounts of lignin on the cellulose

(Fig. 4E). In the cellulose-only samples, 8.8% of the molecules analyzed displayed processive behavior, consistent with previous work (37). With increasing levels of lignification, the processive fraction decreased sharply to a plateau at 1 mM CA, and at 9 mM CA the processive percentage was 1.5%, indicating an 83% reduction of the processive fraction. Run length also decreased from 36.0 ± 2.8 nm (mean ± SEM, N = 224 particles) in the cellulose-only sample to 21.7 ± 2.1 nm (mean ± SEM, N = 56 particles) on lignocellulose made with 9 mM CA, representing a 40% decline (Fig. 4F). The diminished run lengths of the processive enzymes suggest that at least part of the reduction in processive percentage can be explained by their run lengths falling below the 10 nm threshold we established for processive movement. Together, the shorter average run length and reduced fraction of processive enzymes are consistent with lignin acting as a barrier that impedes processive degradation of cellulose by Cel7A.

Finally, the Cel7A velocity, defined as the distance over the duration of processive segments, decreased by roughly half from 3.37 ± 0.25 nm/s (mean ± SEM, N = 224) in the control samples, consistent with previous work (37), to 1.54 ± 0.23 nm/s (mean ± SEM, N = 56) in the 9 mM CA samples (Fig. 4G). Similar to the processive percentage, the velocity fell steeply across the lower CA concentrations, where very little lignin was visible by electron microscopy (e.g., 0.11 mM CA in Fig. 2H). This slowing of Cel7A velocity indicates that, beyond acting as an impediment, lignin affects the ability of Cel7A to processively extract and hydrolyze the cellulose polymer.

Lignin polymerized *in vitro* appears to form a thin layer on the cellulose surface

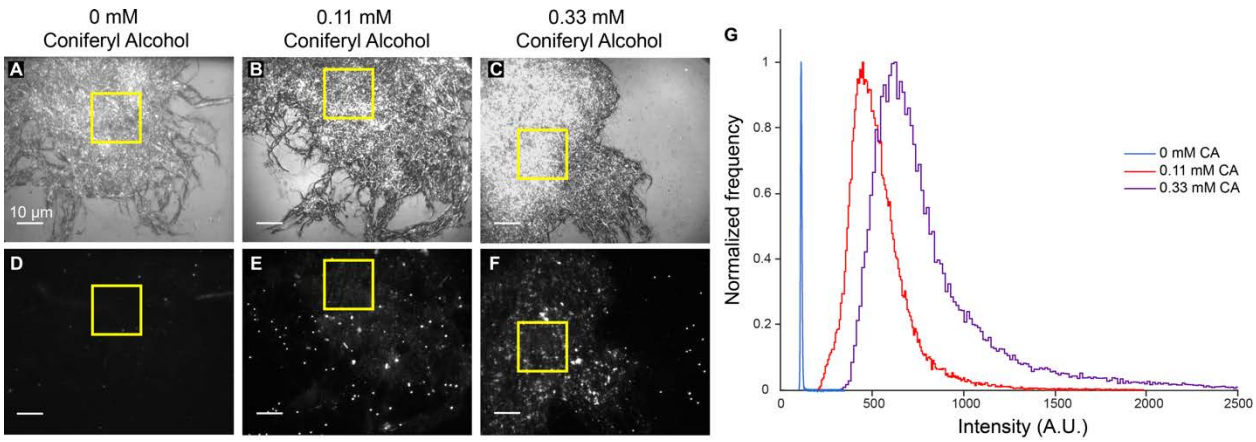

Figure 5: Lignin polymerized *in vitro* with low concentrations of coniferyl alcohol forms a thin layer of lignin that covers the cellulose surface. A-C: lignocellulose adhered to glass surface imaged using interference reflection microscopy; scale bar = 10 µm. D-F: total internal reflection fluorescence microscopy micrographs of lignocellulose stained with the lignin dye Basic Fuchsin; scale bar = 10 µm. G: Distribution of intensity values from Basic Fuchsin signal on lignocellulose surface of cellulose-only sample (blue), 0.11 mM CA lignocellulose sample (red), and 0.33 mM CA lignocellulose sample (purple). The frequency peaks for each sample were normalized to a value of 1 and the x-axis was truncated at 2500 A.U. Yellow squares indicate the 250-pixel by 250-pixel area of cellulose that intensity values were measured. Line scans that show fluorescence intensity across the samples are provided in Fig. S5.

The decrease in the velocity and processive percentage at low CA concentrations where only sparse lignin labeling was observed by SEM raises the possibility that even in these samples there is a thin layer of lignin on the cellulose surface, invisible in SEM, that may slow the hydrolysis of cellulose by Cel7A. To investigate this possibility, we used fluorescence microscopy to test whether at low CA concentrations, lignin polymerizes on the cellulose surface in a form that is undetectable by IRM or SEM. To do this, we labeled lignin with Basic Fuchsin and measured the fluorescence intensity of the control and lightly lignified samples. Flow cells were formed with lignocellulose adhered to the surface of the glass coverslip, Basic Fuchsin was injected into the flow cell and incubated for 5 minutes, and excess dye was removed by extensively

293 washing with sodium acetate buffer. Samples were then imaged using IRM to visualize the
294 cellulose and by TIRFM to measure the fluorescence of Basic Fuchsin-stained lignin. 250-pixel
295 by 250-pixel areas containing a minimal number of bright lignin aggregates were selected (yellow
296 squares in Fig. 5D-F) and a histogram of lignin fluorescence intensities was generated from each
297 sample. Similar labeling, illumination, and camera settings were used to enable quantitative
298 comparison of lignin intensities across different samples.
299
300 In the cellulose-only sample, the Basic Fuchsin signal was negligible (Fig. 5D), with a very
301 narrow distribution of intensities around a peak of 113 A.U. (Fig. 5G). This value is very close the
302 background signal in cellulose-free regions of the coverslip (Fig. S5), indicating that Basic Fuchsin
303 does not label cellulose. In the 0.11 mM and 0.33 mM CA samples, the lignin fluorescence
304 increased across the cellulose surface as seen by eye in Figure 5E-F, and the pixel intensity
305 distribution peaked at 448 A.U. and 621 A.U., respectively (Fig. 5G). The 0.33 mM CA sample
306 contained lignin aggregates, visible by eye in the highlighted region, and these high intensities are
307 apparent in the long tail of the 0.33 mM CA intensity distribution. Notably, there was virtually
308 zero overlap in intensities between the cellulose-only control and the two lignified samples. This
309 lack of overlap suggests that to the resolution of our fluorescence measurements, lignin is present
310 everywhere on the cellulose surface, consistent with lignin forming a thin layer around the
311 cellulose strands that is distinct from the small aggregates observed in the SEM and IRM images
312 in Figure 2.2. This thin lignin layer provides a potential explanation for the slowing of Cel7A even
313 at the lowest CA concentrations where deposition of obvious lignin aggregates is sparse.
314

Discussion

In this work we investigated the potential mechanisms by which lignin inhibits degradation of lignocellulose by the cellulase Cel7A. The data from our model system suggest that lignin does not act as a sink to irreversibly bind cellulases, but instead blocks Cel7A from binding to the cellulose surface, and acts as both an impediment to slow engaged enzymes and as a roadblock to block progress along a cellulose strand.

In vitro polymerized lignin occludes the surface of cellulose

During the assembly of secondary plant cell walls, lignin is thought to polymerize onto cellulose-hemicellulose networks and form layers surrounding the microfibrils, with the degree of lignification depending on the type of biomass (45). While hemicellulose can be removed through various single-step pretreatments, G-lignin has proven to be difficult to fully remove from lignocellulosic biomass (46). High temperature alkaline pretreatment, one of the more effective approaches for lignin removal, alters the interaction between lignin and cellulose and causes lignin to form small aggregates (18, 31, 46-48). On the other hand, some acidic pretreatments cause the lignin to restructure around the cellulose into sheet-like structures (46).

Because we aimed to create lignocellulose samples that serve as a model for the lignocellulosic biomass used in biofuel production, we characterized our samples using SEM, IRM, and fluorescence microscopy. In the absence of lignin, the cellulose samples showed a meshwork of cellulose strands that intertwined with each other to create a complex web-like structure. This structure is roughly analogous to the bundled, multi-lamellate structure of cellulose

in native plant cell walls (49), although cellulose in native walls is also typically interspersed in matrix polysaccharides such as hemicelluloses. Lignin polymerized in the absence of cellulose exhibited cauliflower-like assemblies under SEM, which appeared as high contrast 'blobs' in IRM. By SEM, lignin in the 0.11 mM and 0.33 mM CA samples appeared as small round aggregates in the cellulose meshwork. These structures may be analogous to the aggregates seen following high temperature alkaline pretreatment of native lignocellulose (18, 31, 46). Importantly, we observed Basic Fuchsin staining across the entire cellulose surface in these samples, suggesting that there is a thin coating of lignin across the surface that we do not detect by SEM or IRM. Evidence of lignin forming thin films in contact with cellulose has previously been reported (50, 51). By SEM, lignin in the 1 mM, 3 mM, and 9 mM CA samples appeared as larger and more structured assemblies on the cellulose surface and formed patches that wrapped around cellulose strands and occluded large regions of the cellulose surface (Fig. 2 and Fig. S1). These lignin structures may be analogous to the sheet-like structures seen following acid pretreatment of more highly lignified samples, such as softwood or wheat straw (31, 45).

Cel7A does not accumulate on *in vitro* polymerized lignin

Published work has posited a 'sink' model in which lignin inhibits cellulase activity due to enzymes binding tightly and unproductively to lignin. One line of evidence comes from studies in which Cel7A is combined with cellulose or lignocellulose, the solution pelleted by centrifugation, and the amount of enzyme remaining in the supernatant compared. Diminished Cel7A in the supernatant for lignified cellulose samples was interpreted to mean that Cel7A binds directly to lignin (19, 26, 28, 29). A second line of evidence comes from experiments that measure the

360 enzymatic activity of Cel7A by monitoring cellobiose production and find that activity is reduced
361 in lignified cellulose compared to bare cellulose (13, 19, 26).
362
363 We found in fluorescence colocalization experiments (Fig. 3) that Cel7A does not
364 accumulate on lignin and instead that regions of high lignin density correlate with less Cel7A
365 binding in the presence of BSA. Without the addition of BSA in the samples, no correlation was
366 measured between Cel7A binding and lignin deposition (Fig. S4). These data argue against the
367 idea of lignin acting as a sink. Instead, they support a model of lignin blocking initial adsorption
368 of Cel7A to cellulose by physically covering the cellulose surface. Further, they suggest that the
369 decreased enzymatic activity of Cel7A due to lignin in bulk assays might result from lignin
370 reducing the accessible surface area of cellulose, rather than from Cel7A irreversibly binding to
371 lignin. Consistent with our results, cellulases show only modest binding to lignin in native cell
372 walls in high-resolution microscopy experiments (31). One significant discrepancy between our
373 experiments and previous work in bulk assays is that bulk assays use ~10^3 to 10^4-fold higher
374 enzyme concentrations than the nM concentrations used in our single-molecule studies. Thus, the
375 negative Pearson's correlation we see between cellulose and lignin binding indicates that Cel7A
376 binds more tightly to cellulose than it does to lignin, but it does not rule out some nonspecific
377 binding of Cel7A to lignin at the high enzyme concentrations used in bulk assays. Consistent with
378 this, measured dissociation constants for cellulases binding to purified lignin are orders of
379 magnitudes higher than the enzyme concentrations used in our assays (28, 29). Additionally, lignin
380 in native lignocellulosic biomass is generally comprised of a mixture of monolignols (46), and
381 future work is warranted to investigate whether cellulases bind more tightly to forms of lignin
382 other than our pure synthetic G-lignin.

383

384 ***In vitro* polymerized lignin impedes Cel7A motion on cellulose**

385 It is easy to envision that the large lignin aggregates and patches on the cellulose surface
386 visible by EM (Fig. 2) would disrupt interactions between Cel7A and cellulose, but Cel7A would
387 be expected to interact normally in the microns-scale areas of cellulose that do not contain these
388 large lignin assemblies. Consistent with this, in the 0.11 and 0.33 mM CA samples, the Cel7A run
389 length matched the cellulose-only control (Fig. 4). However, over this CA range both the
390 processive percentage and the velocity decreased steeply (Fig. 4). How could low levels of lignin
391 alter the velocity and processive percentage without affecting the run length? Based on our
392 fluorescence imaging of lignin by Basic Fuchsin, we interpret this inhibition to be due to a thin
393 layer of lignin that coats the cellulose surface and is invisible in IRM and SEM. If the layer of
394 lignin is thin enough to be penetrated or bypassed by the enzyme, the cellulase would still be able
395 to bind to and hydrolyze the cellulose, but it might require more time to extract a cellulose chain
396 from the fibril surface or its movement along the cellulose surface might be impeded, both of
397 which would result in a lower velocity.

398

399 The decline in the processive percentage of Cel7A molecules with increasing lignin content
400 might result from the lignin layer preventing Cel7A from accessing free ends of the cellulose or
401 from extracting a cellulose chain from the crystal lattice. This finding that lignin decreased the
402 percentage of processive Cel7A molecules provides another possible explanation for the reduced
403 activity of Cel7A on lignified cellulose observed in bulk studies – because these static enzymes
404 are likely not processively degrading cellulose, increasing the fraction of static enzymes is
405 expected to decrease the overall catalytic turnover rate of the population of enzymes as measured

406 in bulk. This diminished activity due to a reduced processive percentage would add to the expected
407 reduced activity due to shorter run lengths and slower velocities.
408
409
410 **Conclusions**

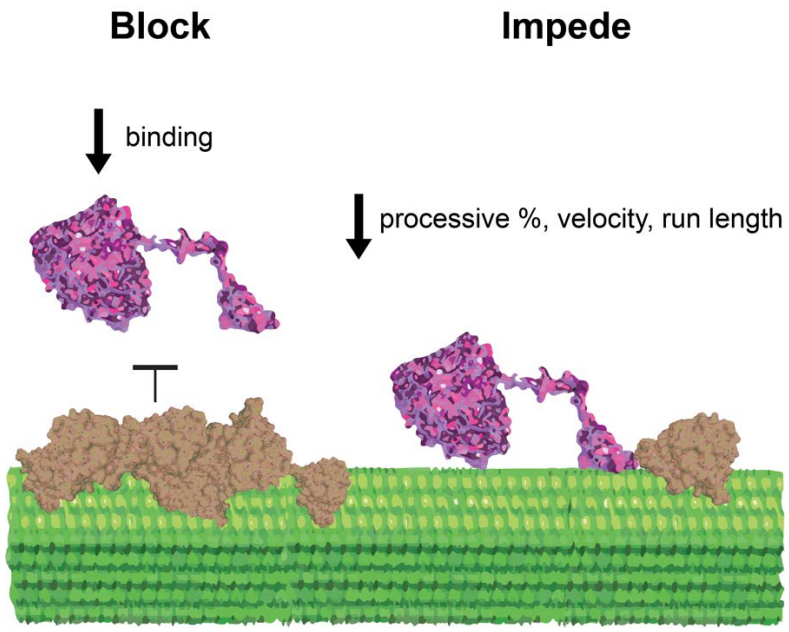

411
412 **Figure 6: Models for Cel7A inhibition on cellulose caused by lignin as supported by single-molecule**
413 **observations.** Lignin covering the cellulose surface prevents Cel7A from binding to the cellulose substrate. Lignin
414 on the cellulose surface can either partially or completely diminish the processive movement of Cel7A on cellulose.
415 Lignin does not act as a sink due to the lack of Cel7A accumulation on lignin.
416
417 Based on the results of this study of a model cellulase and a simplified model for a plant
418 cell wall, we posit two molecular mechanisms to explain the inhibition of Cel7A activity by lignin
419 (Fig. 6). First, we propose that lignin on the cellulose surface impairs Cel7A activity by blocking
420 Cel7A binding to cellulose. Second, we propose that aggregates and patches of lignin act as
421 roadblocks on the cellulase surface that impede Cel7A movement, and at higher degrees of

lignification, the lignin entraps cellulose strands and occludes the cellulose entirely. Third, based on the observation that no Cel7A accumulates on lignin under the conditions tested here, we conclude that lignin does not act as a sink in our system, and instead acts to shield cellulose from Cel7A, such that Cel7A tends to bind to areas of cellulose that are not obstructed by lignin. Finally, based on our observations at low degrees of lignification, we hypothesize that thin films of lignin can cover the cellulose surface and both diminish Cel7A velocity and reduce the percentage of enzymes that undergo processive movement on cellulose.

In extrapolating our findings up to real-world bioenergy applications, a number of caveats should be noted. First, we have chosen our experimental conditions to best enable comparison to published work, and it is possible that changes in pH, ionic strength, temperature, as well as the sources of cellulose and lignin could alter both cellulase activity and lignin-cellulose interactions. Furthermore, cell walls are built in a hierarchical assembly that also includes hemicellulose and pectin, and pretreatment involves varying approaches to removing and modifying the different cell wall components. Thus, future work using lignocellulose from different biological sources and at different stages of treatment is warranted to understand the degree to which the results in our model system are generalizable.

Materials and Methods

Cellulose and lignin preparation and characterization – Bacterial cellulose was produced by inoculating Schramm-Hestrin medium with *Gluconacetobacter hansenii* (strain ATCC 23769) (52), and growing the culture for 5 days at 30°C with no agitation. The resulting sheet of cellulose was washed five times with 100% ethanol. After filtration, 2% (w/v) NaOH was added to the cellulose and the solution was incubated for 30 minutes at 80°C. Next, the solution was centrifuged

445 for 15 min at 2,300 rcf and the supernatant was decanted. The pellet was washed once with 0.5 M
446 sodium acetate and twice with sterile ddH_2O before being air dried for 2 days on aluminum foil.
447 After drying, the cellulose was peeled off and stored at 4°C. Dried cellulose was re-suspended in
448 50 mL ddH_2O and sonicated with a Sonic Dismembrator (Thermo Fisher, model 100) five times
449 for 30 seconds each at a setting of 9, with 1 min breaks in between. Sonicated cellulose samples
450 were combined and processed through a M-110EH microfluidizer at the Pennsylvania State
451 University CSL Behring Fermentation Facility. The sample was first passed through a 200 μm
452 filter five times at 5,000 psi and then passed through a 75 μm filter for 45 minutes at 7,000 psi.
453 The cellulose content was determined by phenol sulfuric acid using a glucose standard (53).
454
455 Lignocellulose samples were created by combining cellulose with coniferyl alcohol (CA),
456 hydrogen peroxide, and horseradish peroxidase (HRP) to polymerize G-lignin on the cellulose
457 surface (38). Two different methods were used to produce the lignin, the first used increasing
458 (HRP) catalyst concentrations proportionally with the hydrogen peroxide and CA concentrations,
459 and the second maintained a constant HRP concentration while the hydrogen peroxide and CA
460 concentrations were increased. Based on the SEM and single-molecule results, both methods of
461 lignin polymerization showed similar effects, so the data were combined into a single data set.
462 Lignin was polymerized by adding 0.11 mM – 9 mM CA and H_2O_2 to 0.5 mL of 4.25 mM
463 acetobacter cellulose along with either 0.01 mg/mL – 0.9 mg/mL HRP for 1 hour at 37°C or 0.01
464 mg/mL HRP for 20 hours at 25°C. The lignocellulose samples were then centrifuged at 9,000 rcf
465 for 5 minutes and gently resuspended in ddH_2O so the final concentration of cellulose was 4.5
466 mM. The removed supernatant was analyzed by measuring the light absorbance at 260 nm to
467 confirm that the oxidation reaction of CA went to completion.

Cel7A preparation and characterization – *T. reesei* Cellobiohydrolase I (Sigma-Aldrich, catalog number: E6412), hereafter referred to as Cel7A, was buffer exchanged into 50 mM sodium acetate using a PD-10 column (General Electric). Peak fractions, as determined by absorbance at 280 nm, were pooled and glycerol was added for a final concentration of 10% (v/v). The final protein concentration (6.02 μM) was determined by light absorbance, using an extinction coefficient of 74,906 $M^{-1}cm^{-1}$. Cel7A was biotinylated using EZ-Link NHS-LC-LC-Biotin (Thermo Scientific, catalog number: 21343), which labels the primary amines of exposed lysine residues. Cel7A was buffer exchanged into 50 mM $NaBO_3$ (pH 8.5), combined with biotin-NHS dissolved in dried Dimethylformamide (DMF) at a biotin:enzyme ratio of 10:1, and incubated for 3 hours in the dark at 21°C. To remove the free biotin, the enzymes were buffer exchanged back into 50 mM sodium acetate using a PD-10 desalting column. The enzyme concentration was calculated using absorbance measurements at 280 nm and the biotin concentration was determined using the Pierce Fluorescence Biotin Quantitation Kit (Thermo Scientific, catalog number: 46610). The biotin:Cel7A ratio was determined to be 0.60. Biotinylated enzymes were flash frozen using liquid nitrogen and stored at -80°C. After thawing for experiments, enzymes were never refrozen.

Single-molecule TIRFM imaging and analysis – To prepare flow cells, a ~10 μL volume of 4.5 mM lignified acetobacter cellulose was pipetted onto the surface of a glass slide, as previously described (37). Two strips of double-sided tape were positioned on either side of the cellulose solution and a plasma cleaned glass cover slip was placed on top of the tape to create a flow cell (~30 μL volume). The slide was inverted and placed into an oven at 65°C for 30 minutes to allow the cellulose solution to dry, leaving the cellulose fibers stuck to the surface of the cover slip.

TetraSpeck beads (Thermo Scientific; catalog number: T7280) used as fiduciary markers were then injected into the flow cell and incubated for 5 minutes to allow them to non-specifically bind to the glass surface. This was followed by three washes of 1 mg/mL bovine serum albumin (BSA) with three minutes incubation each, to prevent nonspecific binding of cellulase enzymes to the glass surface.

Qdot-labeled Cel7A was prepared by mixing 3 nM biotinylated Cel7A with 2 nM Qdot 655 (Thermo Scientific; catalog number: Q10123MP) in 50 mM sodium acetate, pH 5.0, with 5 mM dithiothreitol to prevent photobleaching. Following a 15-minute incubation, the solution was injected into the flow cell. Decreasing the enzyme:particle ratio below this led to many fewer landing events, consistent with Qdots binding single enzymes. Single-molecule imaging was accomplished using total internal reflection fluorescence microscopy (TIRFM) with an excitation laser of 488 nm at 30 mW power to illuminate both the TetraSpeck beads on the surface and the Qdots attached to the enzymes (36). Cellulose was visualized by interference reflectance microscopy (IRM) with a white light LED. Images were taken at 1 frame/s and videos consisted of 1,000 frames. The imaging area for each frame was 79.2 μm x 79.2 μm with a pixel size of 73 nm per pixel. A quadrant photodiode (QPD) sensor connected to the microscope stage prevented drift in the z-direction to keep the images in constant focus. All videos were captured at 21°C.

ImageJ was used to combine two 500-frame videos captured consecutively of the same region of interest to create the final 1,000 frame videos. Videos were analyzed using FIESTA software, which fits two-dimensional Gaussians to the point spread functions of the TetraSpeck beads and the Qdot-labeled cellulases to create single-molecule trajectories (44). The resulting traces were

514 imported into scripts written in MATLAB for further analysis of individual tracks, as described in
515 previous works (36, 37). The positional changes of TetraSpeck beads were subtracted from all
516 tracks to correct for stage drift in the X-Y direction. Particles with total binding durations of less
517 than 10 seconds were not included in the analysis because it was often difficult to differentiate
518 processive segments from spatial variances observed in static segments. Few molecules had
519 binding durations greater than 510 seconds, but those that did were excluded from the analysis, as
520 they were potentially due to irreversible binding by denatured enzymes, and thus were considered
521 outliers.
522
523 **Scanning electron microscopy imaging and analysis** – Lignocellulose samples were washed six
524 times for 5 minutes each using a Millipore 0.2 μm membrane filter starting at 50% ethanol and
525 increasing the ethanol concentration to 60%, 70%, 85%, 95%, and 100% ethanol. A Leica EM
526 CPD300 was used for critical point drying of the lignocellulose on the membrane filter. The dried
527 samples were then mounted onto an aluminum stub with carbon tape and stored in a desiccator at
528 room temperature until the day of experimentation. The samples were sputter coated with ~10 nm
529 of gold-palladium and visualized using a Zeiss SIGMA VP-FESEM at the Pennsylvania State
530 University Huck Institutes of Life Sciences. Images were captured at 90,000x magnification with
531 a EHT of 3 kV using type II secondary electrons.
532
533
534 **Ethics approval and consent to participate**
535 This study did not involve the use of human participants, human material, human data, or
536 vertebrate or invertebrate animals.

Consent for publication

The manuscript includes no images of humans.

Availability of data and materials

Upon publication, data will be made available on a publicly accessible website at Penn State University.

Competing Interest Statement: The authors declare that they have no known competing financial interests or personal relationships that could have appeared to influence the work reported in this paper.

Funding

This work was supported by the Department of Energy Office of Science grant number DE-SC0019065. N.Z was supported in part by a Vaadia-BARD Postdoctoral Fellowship grant number FI-622-2022.

Author Contributions: Z.K.H, D.N, N.Z., M.T., C.T.A. and W.O.H. designed research; Z.K.H. and D.G. performed research; Z.K.H. and D.G. analyzed data; Z.K.H., C.T.A. and W.O.H. wrote the paper.

Acknowledgements

The authors thank members of the Hancock and Anderson labs for support and helpful suggestions and thank Mikaela Meyers for assistance in bacterial cellulose preparation.

References

1. Hill J, Nelson E, Tilman D, Polasky S, Tiffany D. Environmental, economic, and energetic costs and benefits of biodiesel and ethanol biofuels. Proc Natl Acad Sci U S A. 2006;103(30):11206-10.

2. Ruan R, Zhang Y, Chen P, Liu S, Fan L, Zhou N, et al. Biofuels: Introduction. Biofuels: Alternative Feedstocks and Conversion Processes for the Production of Liquid and Gaseous Biofuels2019. p. 3-43.

3. Boerjan W, Ralph J, Baucher M. Lignin biosynthesis. Annu Rev Plant Biol. 2003;54:519-46.

4. Sheehan J, Himmel M. Enzymes, Energy, and the Environment: A Strategic Perspective on the U.S. Department of Energy's Research and Development Activities for Bioethanol. Biotechnol Prog. 1999;15(5):817-27.

5. French AD, Bertoniere NR, Brown RM, Chanzy H, Gray D, Hattori K, et al. Cellulose. Kirk-Othmer Encyclopedia of Chemical Technology 2003.

6. Payne CM, Knott BC, Mayes HB, Hansson H, Himmel ME, Sandgren M, et al. Fungal cellulases. Chem Rev. 2015;115(3):1308-448.

7. Lebo SE, Gargulak JD, McNally TJ. Lignin. Encyclopedia of Polymer Science and Technology2002.

8. Whetten R, Sederoffavb R. Lignin Biosynthesis. 1995;7:1001-13.

9. Muller G, Varnai A, Johansen KS, Eijsink VG, Horn SJ. Harnessing the potential of LPMO-containing cellulase cocktails poses new demands on processing conditions. Biotechnol Biofuels. 2015;8:187.

10. Arantes V, Saddler JN. Access to cellulose limits the efficiency of enzymatic hydrolysis: the role of amorphogenesis. 2010.

11. Fan LT, Lee Y-H, Beardmore DH. Mechanism of the enzymatic hydrolysis of cellulose: Effects of major structural features of cellulose on enzymatic hydrolysis. Biotechnology and Bioengineering. 1980;22(1):177-99.

12. Jeoh T, Ishizawa CI, Davis MF, Himmel ME, Adney WS, Johnson DK. Cellulase digestibility of pretreated biomass is limited by cellulose accessibility. Biotechnol Bioeng. 2007;98(1):112-22.

13. Yang B, Wyman CE. Effect of xylan and lignin removal by batch and flowthrough pretreatment on the enzymatic digestibility of corn stover cellulose. Biotechnol Bioeng. 2004;86(1):88-95.

14. Saini JK, Patel AK, Adsul M, Singhania RR. Cellulase adsorption on lignin: A roadblock for economic hydrolysis of biomass. Renew Energ. 2016;98:29-42.

15. Kellock M, Rahikainen J, Marjamaa K, Kruus K. Lignin-derived inhibition of monocomponent cellulases and a xylanase in the hydrolysis of lignocellulosics. Bioresource Technol. 2017;232:183-91.

16. Cai C, Zhang CF, Li N, Liu HF, Xie J, Lou HM, et al. Changing the role of lignin in enzymatic hydrolysis for a sustainable and efficient sugar platform. Renew Sust Energ Rev. 2023;183:113445.

603 17. Donaldson L, Vaidya A. Visualising recalcitrance by colocalisation of cellulase, lignin and
604 cellulose in pretreated pine biomass using fluorescence microscopy. Sci Rep. 2017;7:44386.
605 18. Huang C, Jiang X, Shen X, Hu J, Tang W, Wu X, et al. Lignin-enzyme interaction: A
606 roadblock for efficient enzymatic hydrolysis of lignocellulosics. Renewable and Sustainable
607 Energy Reviews. 2022;154:111822.
608 19. Strobel KL, Pfeiffer KA, Blanch HW, Clark DS. Structural insights into the affinity of
609 Cel7A carbohydrate-binding module for lignin. J Biol Chem. 2015;290(37):22818-26.
610 20. Baruah J, Nath BK, Sharma R, Kumar S, Deka RC, Baruah DC, et al. Recent Trends in the
611 Pretreatment of Lignocellulosic Biomass for Value-Added Products. Front Energy Res.
612 2018;6:126195.
613 21. Kucharska K, Rybarczyk P, Holowacz I, Lukajtis R, Glinka M, Kaminski M. Pretreatment
614 of Lignocellulosic Materials as Substrates for Fermentation Processes. Molecules.
615 2018;23(11):2937.
616 22. Galbe M, Wallberg O. Pretreatment for biorefineries: a review of common methods for
617 efficient utilisation of lignocellulosic materials. Biotechnology for Biofuels. 2019;12(1):294.
618 23. Mankar AR, Pandey A, Modak A, Pant KK. Pretreatment of lignocellulosic biomass: A
619 review on recent advances. Bioresource Technol. 2021;334:135235.
620 24. Carrard G, Koivula A, Soderlund H, Beguin P. Cellulose-binding domains promote
621 hydrolysis of different sites on crystalline cellulose. Proc Natl Acad Sci U S A.
622 2000;97(19):10342-7.
623 25. Mudinoor AR, Goodwin PM, Rao RU, Karuna N, Hitomi A, Nill J, et al. Interfacial
624 molecular interactions of cellobiohydrolase Cel7A and its variants on cellulose. Biotechnol
625 Biofuels. 2020;13:10.

626 26. Bernardez TD, Lyford K, Hogsett DA, Lynd LR. Adsorption of Clostridium thermocellum
627 cellulases onto pretreated mixed hardwood, avicel, and lignin. Biotechnol Bioeng.
628 1993;42(7):899-907.
629 27. Ishizawa CI, Jeoh T, Adney WS, Himmel ME, Johnson DK, Davis MF. Can delignification
630 decrease cellulose digestibility in acid pretreated corn stover? Cellulose. 2009;16(4):677-86.
631 28. Ooshima H, Burns DS, Converse AO. Adsorption of cellulase from Trichoderma reesei on
632 cellulose and lignacious residue in wood pretreated by dilute sulfuric acid with explosive
633 decompression. Biotechnol Bioeng. 1990;36(5):446-52.
634 29. Palonen H, Tjerneld F, Zacchi G, Tenkanen M. Adsorption of Trichoderma reesei CBH I
635 and EG II and their catalytic domains on steam pretreated softwood and isolated lignin. J
636 Biotechnol. 2004;107(1):65-72.
637 30. Rollin JA, Zhu Z, Sathitsuksanoh N, Zhang YH. Increasing cellulose accessibility is more
638 important than removing lignin: a comparison of cellulose solvent-based lignocellulose
639 fractionation and soaking in aqueous ammonia. Biotechnol Bioeng. 2011;108(1):22-30.
640 31. Zeng Y, Zhao S, Yang S, Ding SY. Lignin plays a negative role in the biochemical process
641 for producing lignocellulosic biofuels. Curr Opin Biotechnol. 2014;27:38-45.
642 32. Liu H, Sun J, Leu S-Y, Chen S. Toward a fundamental understanding of cellulase-lignin
643 interactions in the whole slurry enzymatic saccharification process. Biofuels, Bioproducts and
644 Biorefining. 2016;10(5):648-63.
645 33. Rahikainen JL, Martin-Sampedro R, Heikkinen H, Rovio S, Marjamaa K, Tamminen T, et
646 al. Inhibitory effect of lignin during cellulose bioconversion: the effect of lignin chemistry on non-
647 productive enzyme adsorption. Bioresour Technol. 2013;133:270-8.

34. Tokunaga Y, Nagata T, Suetomi T, Oshiro S, Kondo K, Katahira M, et al. NMR Analysis on Molecular Interaction of Lignin with Amino Acid Residues of Carbohydrate-Binding Module from Trichoderma reesei Cel7A. Sci Rep. 2019;9(1):1977.

35. Chen H, Jiang B, Zou C, Lou Z, Song J, Wu W, et al. Exploring how lignin structure influences the interaction between carbohydrate-binding module and lignin using AFM. Int J Biol Macromol. 2023;232:123313.

36. Nong D, Haviland ZK, Kuntz KV, Tien M, Anderson CT, Hancock WO. Integrated multi-wavelength microscope combining TIRFM and IRM modalities for imaging cellulases and other processive enzymes. Biomed Opt Express. 2021;12(6):3253-64.

37. Haviland ZK, Nong D, Vasquez Kuntz KL, Starr TJ, Ma D, Tien M, et al. Nanoscale dynamics of cellulose digestion by the cellobiohydrolase TrCel7A. J Biol Chem. 2021;297(3):101029.

38. Basu S, Catchmark JM, Brown NR, Anderson CT, Gorniak IP. BcsAB synthesized cellulose on nickel surface: polymerization of monolignols during cellulose synthesis alters cellulose morphology. Cellulose. 2020;27(10):5629-39.

39. Mahamdeh M, Simmert S, Luchniak A, Schaffer E, Howard J. Label-free high-speed wide-field imaging of single microtubules using interference reflection microscopy. J Microsc. 2018;272(1):60-6.

40. Simmert S, Abdosamadi MK, Hermsdorf G, Schäffer E. LED-based interference-reflection microscopy combined with optical tweezers for quantitative three-dimensional microtubule imaging. 2018;26:14499.

669 41. Kapp N, Barnes WJ, Richard TL, Anderson CT. Imaging with the fluorogenic dye Basic
670 Fuchsin reveals subcellular patterning and ecotype variation of lignification in Brachypodium
671 distachyon. J Exp Bot. 2015;66(14):4295-304.
672 42. French AP, Mills S, Swarup R, Bennett MJ, Pridmore TP. Colocalization of fluorescent
673 markers in confocal microscope images of plant cells. Nat Protoc. 2008;3(4):619-28.
674 43. Sedgwick P. Pearson's correlation coefficient. Brit Med J. 2012;344:e4483.
675 44. Ruhnow F, Zwicker D, Diez S. Tracking single particles and elongated filaments with
676 nanometer precision. Biophysical journal. 2011;100(11):2820-8.
677 45. Faik A. “Plant Cell Wall Structure-Pretreatment” the Critical Relationship in Biomass
678 Conversion to Fermentable Sugars. In: Gu T, editor. Green Biomass Pretreatment for Biofuels
679 Production. Dordrecht: Springer Netherlands; 2013. p. 1-30.
680 46. Ong RG, Chundawat SPS, Hodge DB, Keskar S, Dale BE. Linking Plant Biology and
681 Pretreatment: Understanding the Structure and Organization of the Plant Cell Wall and Interactions
682 with Cellulosic Biofuel Production. In: McCann MC, Buckeridge MS, Carpita NC, editors. Plants
683 and BioEnergy. New York, NY: Springer New York; 2014. p. 231-53.
684 47. Koo BW, Min BC, Gwak KS, Lee SM, Choi JW, Yeo H, et al. Structural changes in lignin
685 during organosolv pretreatment of Liriodendron tulipifera and the effect on enzymatic hydrolysis.
686 Biomass Bioenerg. 2012;42:24-32.
687 48. Donohoe BS, Decker SR, Tucker MP, Himmel ME, Vinzant TB. Visualizing Lignin
688 Coalescence and Migration Through Maize Cell Walls Following Thermochemical Pretreatment.
689 Biotechnology and Bioengineering. 2008;101(5):913-25.

690 49. Zhang T, Zheng YZ, Cosgrove DJ. Spatial organization of cellulose microfibrils and matrix
691 polysaccharides in primary plant cell walls as imaged by multichannel atomic force microscopy.
692 Plant J. 2016;85(2):179-92.
693 50. Farooq M, Zou T, Valle-Delgado JJ, Sipponen MH, Morits M, Osterberg M. Well-Defined
694 Lignin Model Films from Colloidal Lignin Particles. Langmuir. 2020;36(51):15592-602.
695 51. Micic M, Radotic K, Jeremic M, Leblanc RM. Study of Self-Assembly of the Lignin Model
696 Compound on Cellulose Model Substrate. Macromolecular Bioscience. 2003;3(2):100-6.
697 52. Hestrin S, Schramm M. Synthesis of Cellulose by Acetobacter-Xylinum. 2. Preparation of
698 Freeze-Dried Cells Capable of Polymerizing Glucose to Cellulose. Biochem J. 1954;58(2):345-
699 52.
700 53. Dubois M, Gilles KA, Hamilton JK, Rebers PA, Smith F. Colorimetric Method for
701 Determination of Sugars and Related Substances. 1956;28:350-6.
702

Lignin impairs Cel7A degradation of in vitro lignified cellulose by impeding enzyme movement and not by acting as a sink

Zachary K. Haviland, Daguan Nong, Nerya Zexer, Ming Tien, Charles T. Anderson, William O. Hancock

Supplemental Figures

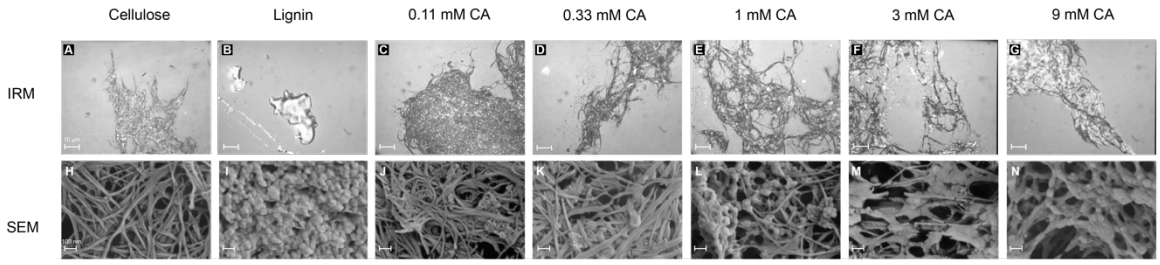

Figure S1 (Related to Figure 2): All CA concentrations used in data set for lignin polymerized onto acetobacter cellulose *in vitro*. First column: cellulose only; second column: lignin only. Third through fifth columns: cellulose with lignin polymerized from different concentrations of CA. Top row are interference reflection micrographs, scale bar = 10 μm. Bottom row are scanning electron micrographs, scale bar = 100 nm.

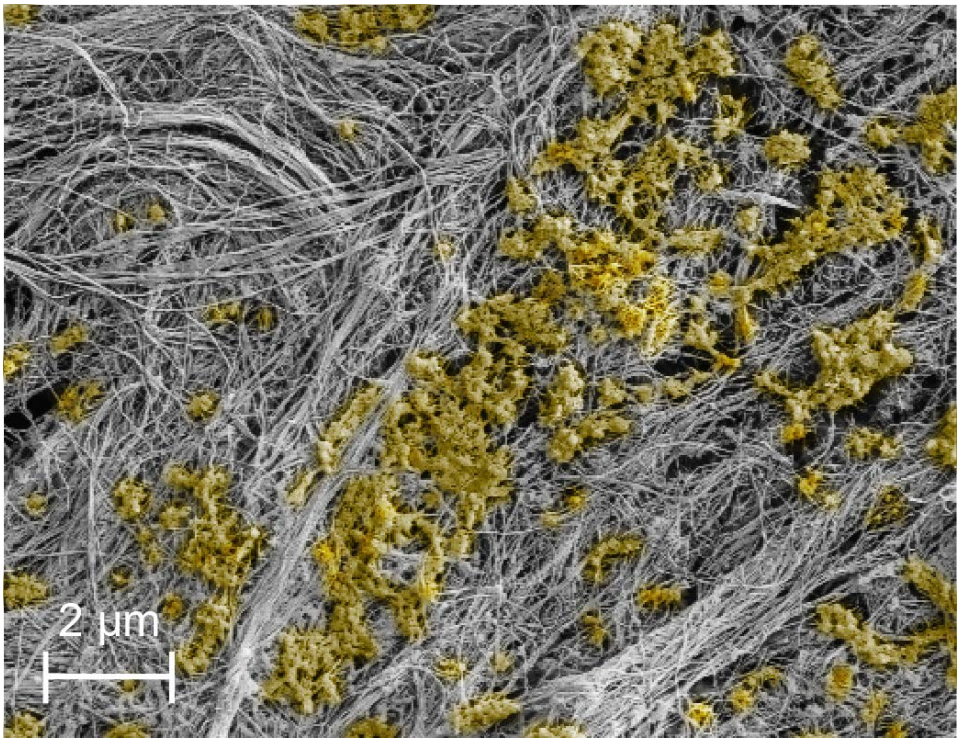

Figure S2 (Related to Figure 2): Lignin generated *in vitro* deposits heterogeneously onto acetobacter cellulose. Scanning electron micrograph of 3 mM CA sample, with lignin false-colored yellow. Areas in the middle of the image display highly lignified regions of cellulose with sheets of lignin (shown in yellow) covering significant areas of the cellulose surface In contrast, areas in the upper left and bottom right of the image contain less lignin on the cellulose surface, with some regions appearing to have nearly no visible lignin and appearing similar to the cellulose-only samples.

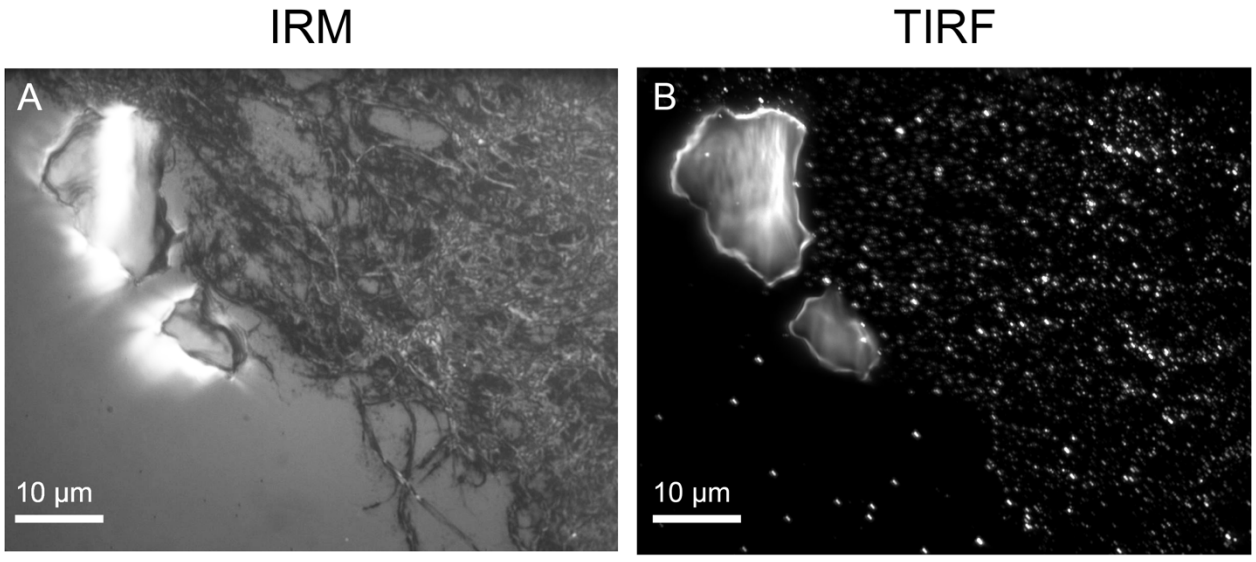

Figure S3: Pure in vitro polymerized lignin has similar Cel7A binding properties to lignin polymerized onto cellulose. Lignin was polymerized in the absence of cellulose, following the same procedures as the lignocellulose samples. A drop of lignin solution and a drop of purified cellulose solution were then placed together onto a glass slide. A flow cell was constructed and placed inverted in an oven at 65°C for 30 minutes to dry the lignin and cellulose onto the cover slip, and then BSA was flowed into the chamber to prevent nonspecific binding of Cel7A to the glass surface. Qdot-labeled Cel7A was then injected into the flow cell, binding locations were visualized for 500 seconds in TIRF, and then Basic fuchsin was introduced to fluorescently label the lignin. An image of Cellulose and lignin visualized via IRM is shown on the left (panel A), and an image of Qdot-labeled Cel7A and fluorescently-labeled lignin visualized by TIRF is shown in the right (panel B). Note that Cel7A preferentially binds to the cellulose with minimal binding to the lignin.

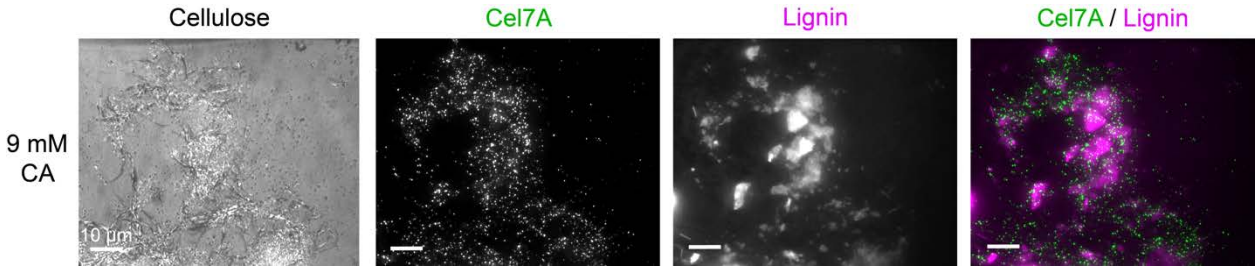

Figure S4 (Related to Figure 3): BSA reduces the binding of Cel7A to lignin. 9 mM CA lignocellulose was adsorbed to the slide without the addition of BSA to the flow cell to determine if BSA affects Cel7A binding to lignin. Binding locations of Qdot-labeled Cel7A were recorded for 50 seconds before being washed out and Basic Fuchsin was added to determine locations of lignin deposition. A Pearson's correlation coefficient of 0.037 was calculated, as described in Methods. This value indicates no correlation between Cel7A binding and lignin, which differs from previous results with BSA added to the flow cell as shown in Figure 3. This shows the BSA washes may affect the Cel7A binding to lignin, but the lignin still does not appear to act as a sink where a larger positive correlation would be expected.

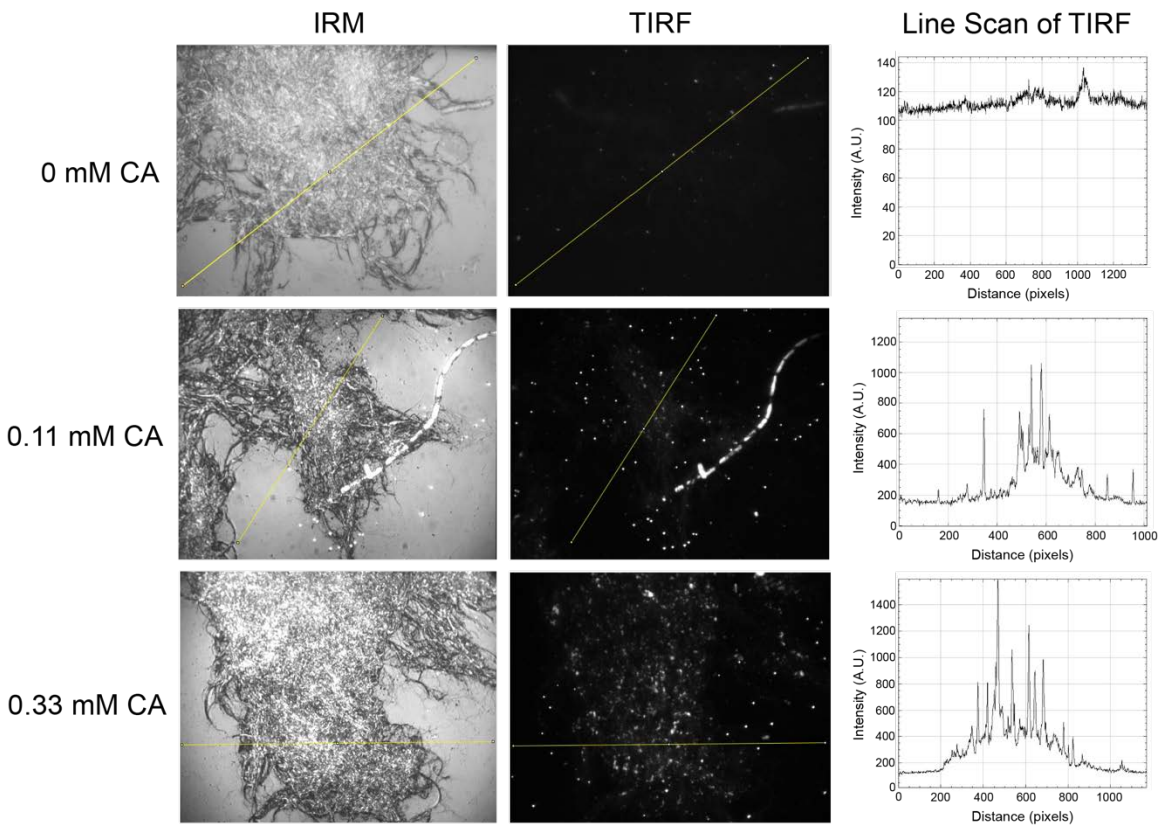

Figure S5 (Related to Figure 5): Line scans across the lignocellulose surfaces show an increase in Basic Fuchsin fluorescent signal in the TIRF channels on the lignified cellulose samples compared to cellulose-only samples. Yellow lines in the IRM and TIRF images show the location of the line scan for each sample. The fluorescence intensity across the cellulose surface for the cellulose-only sample is similar to the intensity on the glass surface, indicating no lignin is present in the sample. The 0.11 mM and 0.33 mM CA samples display an increase in fluorescence intensity across the lignocellulose surface compared to the glass surface, signifying the presence of a thin film of lignin on the cellulose surface. The line scans for the lignified samples also show periodic spikes, corresponding to lignin aggregates that can be seen by eye in the fluorescence image.